

Impact of interstitial oxygen on the electronic and magnetic structure in superconducting $\text{Fe}_{1+y}\text{TeO}_x$ thin films

Hefei Hu,^{1,2,*} Ji-Hwan Kwon,^{2,3} Mao Zheng,^{1,2} Can Zhang,^{1,2} Laura H. Greene,^{1,2} James N. Eckstein,^{1,2} and Jian-Min Zuo^{2,3,†}

¹*Department of Physics, University of Illinois at Urbana-Champaign, Urbana, Illinois 61801, USA*

²*Frederick Seitz Materials Research Laboratory, University of Illinois at Urbana-Champaign, Urbana, Illinois 61801, USA*

³*Department of Materials Science and Engineering, University of Illinois at Urbana-Champaign, Urbana, Illinois 61801, USA*

(Received 10 June 2014; published 19 November 2014)

Interstitial oxygen critical to the emergence of superconductivity in $\text{Fe}_{1+y}\text{TeO}_x$ thin films has been detected. Its location and concentration are measured by atomic-resolution electron-energy-loss spectroscopy with $x = 0.09$. The density functional theory calculations show that oxygen incorporation leads to local disorder in the magnetic moments of Fe, hole doping by oxygen forming ionic bonds with Fe, and a large magnetic- and position-dependent increase or reduction in the Te-Fe-Te bond angles. An examination of bonding based on charge density further reveals covalent charge between Fe and Te, and its reduction with O doping.

DOI: [10.1103/PhysRevB.90.180504](https://doi.org/10.1103/PhysRevB.90.180504)

PACS number(s): 74.62.Dh, 68.37.Ma, 74.20.Pq, 74.70.Xa

Superconductivity is observed in the $\text{Fe}_{1+y}\text{TeO}_x$ thin films with T_c close to 12 K after oxygen incorporation [1–6]. Oxygen substitutes Te through the introduction of oxygen during film growth [1,4,6] or occupies an interstitial site by oxygen annealing or by exposing to air after film growth [2–6]. The controlled experiment by Zheng *et al.* shows that interstitial oxygen, rather than oxygen substitution, is responsible for the emergence of superconductivity [6]. However, interstitial oxygen is difficult to detect and consequently its impact on the electronic and magnetic structure of $\text{Fe}_{1+y}\text{TeO}_x$ thin films is largely unknown. Since oxygen doping is directly behind the emergence of superconductivity in the $\text{Fe}_{1+y}\text{TeO}_x$ thin films, understanding the exact roles of interstitial oxygen can have a significant impact on our understanding of superconductivity in this materials system.

Fe_{1+y}Te belongs to the 11 family of known Fe chalcogenide crystal structures with the high- T symmetry of $P4/nmm$ [7]. Previous theoretical studies suggested several potential interstitial sites for the interstitial oxygen [3,8,9]. However, no direct evidence of interstitial oxygen has been reported so far. The amount of oxygen in the superconducting thin films is also unknown. X-ray absorption spectroscopy measurements indicated that the Fe valence increased from 2+ to mainly 3+ with oxygen incorporation [2,3]. This suggests a substantial amount of oxygen in the superconducting $\text{Fe}_{1+y}\text{TeO}_x$ thin films.

Here, we report a combined experimental and theoretical study to quantify interstitial oxygen and determine its electronic structure. The Fe_{1+y}Te thin films were grown on the $\text{LaAlO}_3(001)$ substrate by molecular beam epitaxy (MBE) following details reported before [6]. The films were characterized by scanning transmission electron microscopy (STEM) combined with electron-energy-loss spectroscopy (EELS) and x-ray diffraction. Density functional theory (DFT) calculations are used to model the atomic structures with

oxygen incorporation, and investigate the impact of oxygen on the electronic structures for different magnetic configurations.

Superconductivity in the Fe_{1+y}Te thin films emerges with oxygen doping. However, some films remain nonsuperconducting even with the oxygen treatment; these films have a much higher excess Fe content due to a change in the Fe/Te flux ratio in the MBE growth. Two representative superconducting and nonsuperconducting films of 20 and 100 nm thickness, respectively, were selected for study. A comparison of the typical $R(T)$ curves of superconducting and nonsuperconducting films is made in Fig. 1(a). The superconducting films have an onset and zero resistance transition temperatures at ~ 13 and 11 K, respectively [6]. The reduction in resistivity as temperature decreases is broadened, which implies a softened magnetic transition [10]. In contrast, the anomaly at ~ 65 K in the $R(T)$ curve of the nonsuperconducting film is similar to that of bulk crystals, which has been attributed to a sharp magnetic and structural transition in this material [7,11,12]. The two films were characterized by x-ray diffraction. Based on the measured lattice constants and using the reported reference [13], we estimated $\sim 4\%$ excess Fe in the superconducting film ($c \sim 6.32 \text{ \AA}$) and $\sim 18\%$ excess Fe in the nonsuperconducting film ($c \sim 6.26 \text{ \AA}$). Thus, there is a strong correlation between the magnetic properties of Fe_{1+y}Te with the amount of excess Fe [14].

Figure 1(b) shows an atomic-resolution high-angle annual dark-field (HAADF) STEM image recorded along the a axis of the superconducting film. The film is atomically flat on the LaAlO_3 substrate. At the interface, additional atomic layers are sometimes observed between the FeTe film and the substrate, which most likely consist of Fe. To examine whether the film is strained, we performed nanoarea electron diffraction with a probe of 40 nm in diameter centered at the interface. The electron diffraction results show that the (200) reflections from the substrate and film are well separated, as seen in Fig. 1(c), indicating no obvious film strain in agreement with the x-ray reciprocal space mapping result [6]. To detect interstitial oxygen, EELS spectra were recorded along the line indicated in the inset of Fig. 2(b) at an interval distance of 0.74 Å . The experiment was performed on the JEOL2200FS at the University of Illinois, equipped with a CEOS probe

*Present address: Intel Corporation, Folsom, California 95630, USA.

†Corresponding author: jianzuo@illinois.edu

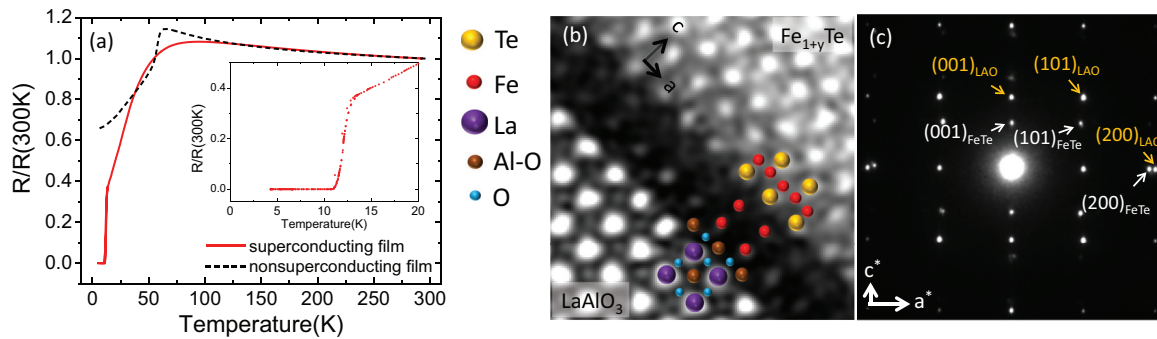


FIG. 1. (Color online) (a) Temperature dependence of resistivity for the superconducting and nonsuperconducting films. The inset shows an onset and zero resistance transition temperature of ~ 13 and 11 K, respectively, for the superconducting film. (b) Atomic-resolution HAADF-STEM image of a FeTe thin film with atomic columns labeled. (c) Electron diffraction pattern recorded from a 40-nm-diameter area centered at the film interface.

corrector and an in-column Ω -energy filter [15]. Figure 2(a) shows an EELS spectrum from the $\text{Fe}_{1+y}\text{Te}_x$ thin film. The O-K edge together with the Te- $M_{4,5}$ and Fe- $L_{2,3}$ edges with the onset energy at ~ 530 , 570 , and 708 eV, respectively, are clearly recorded. The O-K edge integrated intensity after background subtraction using the power-law model is plotted as a function of the probe position in Fig. 2(b). A clear modulation of oxygen distribution is observed from this analysis. For reference, we simultaneously recorded the HAADF intensity during the

EELS acquisition, which is also plotted. The HAADF intensity peaks come from the Te atomic columns due to its large Z . Based on this, the Fe positions can be identified. The comparison between the two curves shows that oxygen signal is peaked next to the Fe atomic plane.

To estimate the amount of interstitial oxygen, the O-K edge was quantified together with the Te- $M_{4,5}$ edge. The background of each signal was determined ~ 40 eV before the edge threshold using the power-law model. Each signal was integrated with a width of 35 eV from the edge threshold. Results show $x = 9 \pm 2\%$ for oxygen in the superconducting thin film. Together with the estimate of 4% excess Fe, the overall composition was determined to be $\text{Fe}_{1+0.04}\text{Te}_{0.09\pm 0.02}$. Thus the amount of interstitial oxygen is substantially larger than the amount of excess Fe in the superconducting film.

The recorded O-K edge shows fine structures with a prepeak at ~ 531 eV and a main peak at ~ 538 eV. The O-K fine structure (see Supplemental Material, Fig. S1 [16]) is similar to the one we previously recorded in oxygen-annealed $\text{Fe}_{1.08}\text{Te}_{0.55}\text{Se}_{0.45}$, which can be interpreted as a mixture of the O-K edges in FeO and $\alpha\text{-Fe}_2\text{O}_3$ [17].

To further determine the position of interstitial oxygen, as well as to study the effects of oxygen doping on the FeTe atomic and magnetic structures, DFT calculations were performed. Both WIEN2K [18] and VASP [19–21] packages were used to perform DFT calculations, and they led to consistent results. In what follows, only the WIEN2K results are presented. The calculations were performed within the generalized gradient approximation (GGA). The experimental lattice constants, $a = 3.821$ Å and $c = 6.285$ Å, were employed for the calculation [22]. A separate calculation using $c = 6.32$ Å, as determined by x-ray diffraction, showed little changes in the results. A $2 \times 2 \times 1$ supercell was used for modeling as shown in Fig. 3(a) and the k -point mesh was an $4 \times 4 \times 5$. All atoms were free to move until the force tolerance of 1 mRy/bohr was reached. Oxygen was placed at the interstitial site above the center of the Fe square lattice based on our EELS evidence, at the opposite side of Te [see Fig. 3(a)], corresponding to the composition of $\text{FeTeO}_{0.125}$. The z height of oxygen was initially set to make the Fe-O bond length at 2 Å, corresponding to the bond distance expected for iron oxides. The relaxed structure is shown in Fig. 3. The oxygen after relaxation is at the top of a pyramidlike structure

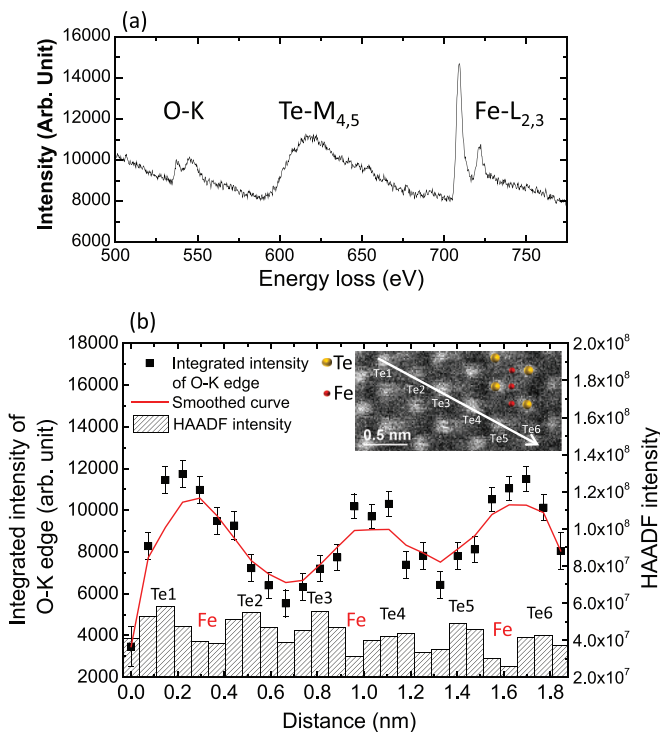


FIG. 2. (Color online) Line-scan EELS analysis of interstitial oxygen. (a) A typical EELS spectrum with O-K, Te- $M_{4,5}$ and Fe- $L_{2,3}$ edges labeled. (b) The integrated intensity of O-K is plotted by solid squares as a function of the scan path shown by the HAADF-STEM image in the inset. Error bars were estimated by assuming Poisson noise distribution for the signal and considering the standard deviation of the background intensity of the O-K. The corresponding smoothed curve is shown in red. The simultaneously recorded HAADF intensity along the scan path is shown below.

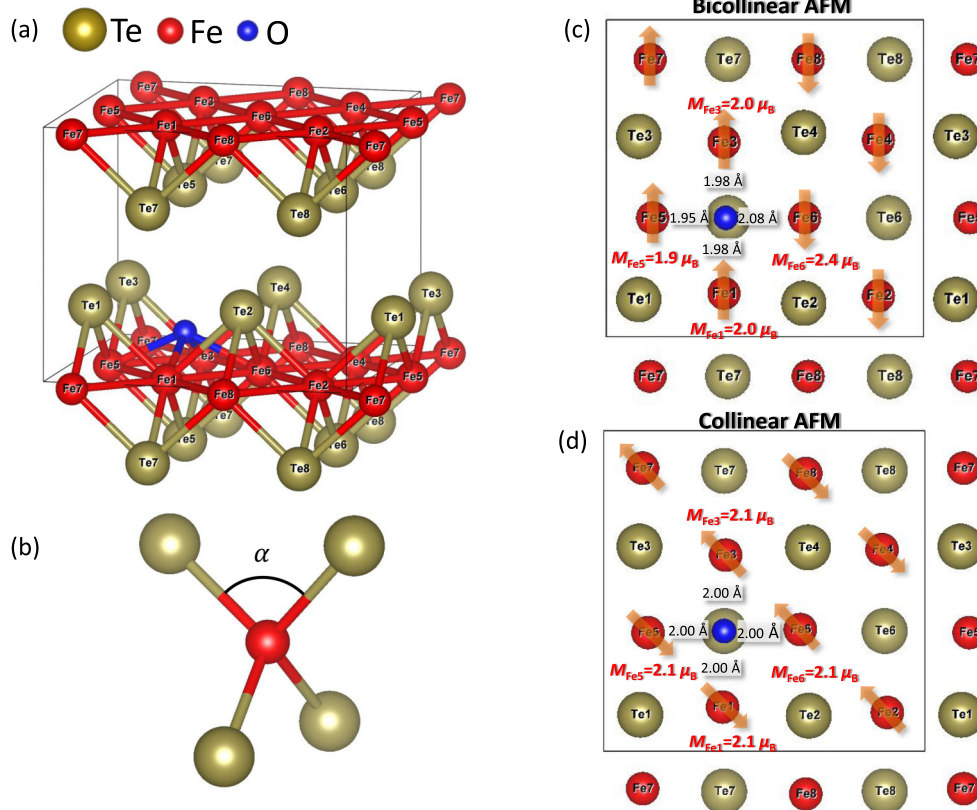


FIG. 3. (Color online) Structural models obtained from DFT calculations. A $2 \times 2 \times 1$ supercell used for modeling is shown in (a) with Te-Fe-Te angle, α , defined in (b). Bicollinear and collinear AFM configurations are shown in (c) and (d), respectively, with calculated Fe-O bond lengths and magnetic moments of Fe ions bonded with oxygen.

with four Fe atoms at the base. We also considered the case that oxygen is centered within the Fe square lattice [8], but the oxygen atom at this location was unstable in agreement with previous reports [3,9]. The calculation here did not include excess Fe. The impact of excess Fe is discussed separately later, based on the DFT calculation results.

The ground state of FeTe is reported to be a bicollinear anti-ferromagnetic (AFM) structure [14,23–25]. For our modeling of $\text{FeTe}_{0.125}$, nonmagnetic, collinear AFM and bicollinear AFM structures [25] were all considered. The spin configurations of bicollinear and collinear AFM are shown in Figs. 3(c) and 3(d), respectively. After atomic relaxation, the total energy of nonmagnetic structure is found to be about 0.29 eV/Fe higher than the other two AFM configurations. For the two AFM structures considered, the bicollinear configuration is lower in energy by 16 meV/Fe.

For FeTe with the bicollinear and collinear AFM structures, the Fe magnetic moment is calculated as $2.3 \mu_B$ and $2.0 \mu_B$, respectively. With oxygen in the bicollinear AFM structure, we obtained for Fe ions next to oxygen, $M_{\text{Fe}1} = M_{\text{Fe}3} = 2.0 \mu_B$, $M_{\text{Fe}5} = 1.9 \mu_B$, and $M_{\text{Fe}6} = 2.4 \mu_B$ (the sites are labeled as Fe1–Fe8 in Fig. 3). The other four Fe atoms have magnetic moments varying from $2.0 \mu_B$ to $2.2 \mu_B$. Notably, the magnetic disorder is accompanied with changes in the Fe-O bond length with $d_{\text{Fe}5-\text{O}} = 1.95 \text{ \AA}$, $d_{\text{Fe}6-\text{O}} = 2.08 \text{ \AA}$, and $d_{\text{Fe}1-\text{O}} = d_{\text{Fe}3-\text{O}} = 1.98 \text{ \AA}$. In comparison, in the collinear AFM structure $M_{\text{Fe}} = 2.1 \mu_B$ is obtained for all four oxygen-

bonded Fe ions, and $2.0 \mu_B$ for the other four Fe ions inside the supercell. Furthermore, the Fe-O bond lengths are found to be the same (2.00 \AA) in the collinear AFM structure. Thus, large magnetic disorder is found only in the oxygen incorporated bicollinear AFM structure.

The bond angle of Te-Fe-Te, α [see Fig. 3(b)], is also impacted by oxygen doping dependent on the magnetic structure. Previous work has shown that T_c increases as α increases with Se doping in $\text{FeTe}_{1-x}\text{Se}_x$ [26]. For FeTe in the bicollinear and collinear AFM structure, α is calculated to be $96.2^\circ/94.7^\circ$ and 97.1° , respectively. Note that two bond angles in the bicollinear AFM structure are the result of structural distortion due to the lattice-magnetic interaction, which was also previously reported [23,27]. With interstitial oxygen, large changes in α are introduced. Changes in α in the bicollinear AFM case range from 0.2° to 6.2° . For a list of α values, see Table S1 in the Supplemental Material [16].

Bond distances and angles, in general, are determined by chemical bonding. To further examine how oxygen impacts bonding and the related electronic structure, we plot the difference charge density maps of FeTe and $\text{FeTe}_{0.125}$ for different spin configurations in Fig. 4. The difference charge density map is calculated as $\Delta\rho = \rho_{\text{crystal}} - \rho_{\text{atoms}}$ where ρ_{crystal} is the calculated charge density and ρ_{atoms} is the superimposed atomic charge density. For FeTe, the difference map shows Fe ions with negative $\Delta\rho$ with d -orbital features, whereas Te ions are polarized with positive $\Delta\rho$ away from the

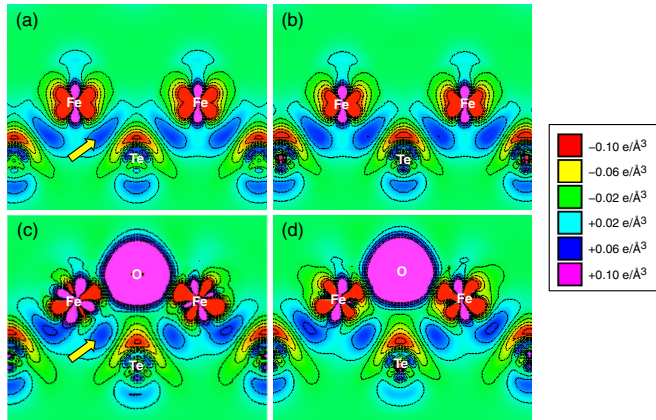


FIG. 4. (Color online) Difference charge density map of (a) FeTe bicollinear AFM, (b) FeTe collinear AFM, (c) FeTeO bicollinear AFM, and (d) FeTeO collinear AFM. Contour interval: $0.02 e/\text{\AA}^3$.

Fe plane. Significantly, there is an electron-accumulated region between Fe and Te, showing a strong covalent feature of the Fe-Te bonding with $\Delta\rho_{\text{Max}} = 0.055 e/\text{\AA}^3$. In FeTeO_{0.125}, the oxygen shows large positive $\Delta\rho$ as a negative ion, forming an ionic bond with Fe. Notably, the electron-accumulated region of the Fe-Te bond has $\Delta\rho_{\text{Max}} = 0.053 e/\text{\AA}^3$, indicating a weakening of the Fe-Te bond by interstitial oxygen. In addition, the polarization of Te underneath the oxygen also changes, showing a reduced polarization compared to the other Te ions. After oxygen incorporation, the *d*-orbital feature of Fe is also slightly rotated, resulting from modification of the electronic structure in the *d* orbital. Since it has been suggested that the strong electronic polarizability of anion plays a crucial role in superconductivity in Fe-based superconductors [28], the bond modifications revealed here are noteworthy.

The effects of excess Fe are further studied by DFT calculations. A $2 \times 2 \times 1$ supercell with one excess Fe was employed for modeling, corresponding to Fe_{1+0.125}Te. The initial excess Fe site was set according to the previous study [29]. Its height is calculated at 1.78 Å (1.65 Å and 1.66 Å for the bicollinear and collinear magnetic configurations, respectively) from the Fe layer, in agreement with previous reports [29,30]. Figure 5 shows the calculated (100) plane difference charge density maps of FeTe and FeTe with the excess Fe. The excess Fe is positively charged as evidenced by its large negative $\Delta\rho$. Positive $\Delta\rho$ is seen between the excess and host Fe atoms, in a covalentlike feature with $\Delta\rho_{\text{Max}}$ at the largest when the spins of the two Fe atoms are the same. The Fe-Te bonding weakens somewhat as measured by $\Delta\rho_{\text{Max}}$. In addition, ionic bonding between the excess Fe and the Te ions modifies the charge density of Te and its polarizability. Near the excess

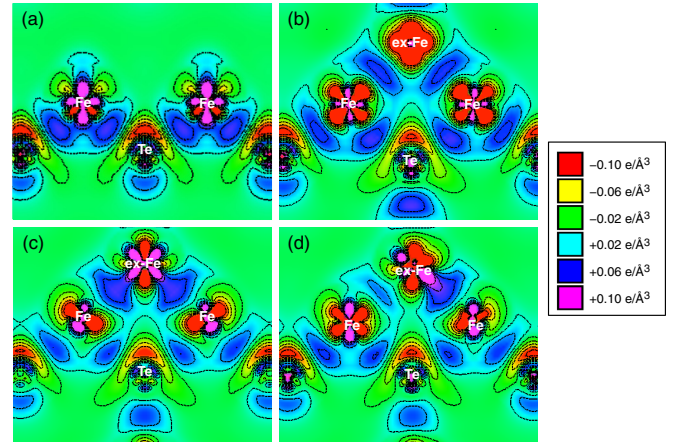


FIG. 5. (Color online) The effects of excess Fe on bonding as observed in the difference charge density maps of the (100) plane for pure FeTe (a) and Fe_{1.125}Te with nonmagnetic (b), bicollinear (c), and collinear (d) AFM magnetic structure. Contour interval: $0.02 e/\text{\AA}^3$.

Fe, the Fe-Fe bond distances are also modified by a small amount, for example, $d_{\text{Fe1-Fe6}}$ decreases from 2.70 Å to 2.64 Å with the excess Fe. Full details are summarized in Tables S2 and S3 in the Supplemental Material [16]. The excess Fe is spin polarized [29]. The magnetic moment of the excess Fe is $2.3\mu_B$, $2.4\mu_B$, and $2.3\mu_B$ for the nonmagnetic, collinear AFM, and bicollinear AFM FeTe, respectively. Overall, the excess Fe contributes to electron doping, a strong magnetic moment, and localized modification of bonding and related bond lengths.

In summary, we have demonstrated oxygen preferentially occupies the interstitial site, bonded to the Fe layer in a pyramidlike configuration. DFT calculations show that there are four major roles of interstitial oxygen in the emergence of superconductivity: (1) hole doping by oxygen that forms ionic bonds with Fe, (2) disruption of long-range AFM order by oxygen-induced magnetic disorder in the bicollinear AFM structure, (3) increase of Te-Fe-Te bond angles in some cases and reduction in other cases, and (4) weakening of the Fe-Te bond. The large magnetic disorder with Fe in the bicollinear AFM state is accompanied by variations in the Fe-O bond lengths, while the interaction of oxygen with Fe in the collinear AFM state leads to smaller variations. In contrast, excess Fe contributes to electron doping, a strong magnetic moment, and smaller variations in the Fe-Fe bond lengths.

This material is based upon work supported as part of the Center for Emergent Superconductivity, an Energy Frontier Research Center funded by the U.S. Department of Energy, Office of Science, Office of Basic Energy Sciences, under Award No. DE-AC0298CH10886.

[1] W. D. Si, Q. Jie, L. J. Wu, J. Zhou, G. D. Gu, P. D. Johnson, and Q. Li, *Phys. Rev. B* **81**, 092506 (2010).

[2] Y. F. Nie, D. Telesca, J. I. Budnick, B. Sinkovic, and B. O. Wells, *Phys. Rev. B* **82**, 020508(R) (2010).

- [3] Y. F. Nie, D. Telesca, J. I. Budnick, B. Sinkovic, R. Ramprasad, and B. O. Wells, *J. Phys. Chem. Solids* **72**, 426 (2011).
- [4] Q. Li, W. D. Si, and I. K. Dimitrov, *Rep. Prog. Phys.* **74**, 124510 (2011).
- [5] D. Telesca, Y. Nie, J. I. Budnick, B. O. Wells, and B. Sinkovic, *Phys. Rev. B* **85**, 214517 (2012).
- [6] M. Zheng, H. Hu, C. Zhang, B. Mulcahy, J.-M. Zuo, and J. Eckstein, *arXiv:1301.4696*.
- [7] K.-W. Yeh, T.-W. Huang, Y.-L. Huang, T.-K. Chen, F.-C. Hsu, P. M. Wu, Y.-C. Lee, Y.-Y. Chu, C.-L. Chen, J.-Y. Luo, D.-C. Yan, and M.-K. Wu, *Europhys. Lett.* **84**, 37002 (2008).
- [8] K. Palandage, G. W. Fernando, Kun Fang, and A. N. Kocharian, *J. Mater. Sci.* **47**, 7671 (2012).
- [9] Z. T. Zhang, Z. R. Yang, W. J. Lu, X. L. Chen, L. Li, Y. P. Sun, C. Y. Xi, L. S. Ling, C. J. Zhang, L. Pi, M. L. Tian, and Y. H. Zhang, *Phys. Rev. B* **88**, 214511 (2013).
- [10] Y. Han, W. Y. Li, L. X. Cao, X. Y. Wang, B. Xu, B. R. Zhao, Y. Q. Guo, and J. L. Yang, *Phys. Rev. Lett.* **104**, 017003 (2010).
- [11] M. H. Fang, H. M. Pham, B. Qian, T. J. Liu, E. K. Vehstedt, Y. Liu, L. Spinu, and Z. Q. Mao, *Phys. Rev. B* **78**, 224503 (2008).
- [12] Y. Mizuguchi, F. Tomioka, S. Tsuda, T. Yamaguchi, and Y. Takano, *J. Phys. Soc. Jpn.* **78**, 074712 (2009).
- [13] Y. Mizuguchi, K. Hamada, and O. Miura, *Phys. Procedia* **27**, 9 (2012).
- [14] W. Bao, Y. Qiu, Q. Huang, M. A. Green, P. Zajdel, M. R. Fitzsimmons, M. Zhernenkov, S. Chang, M. Fang, B. Qian, E. K. Vehstedt, J. Yang, H. M. Pham, L. Spinu, and Z. Q. Mao, *Phys. Rev. Lett.* **102**, 247001 (2009).
- [15] J. G. Wen, J. Mabon, C. H. Lei, S. Burdin, E. Sammann, I. Petrov, A. B. Shah, V. Chobpattana, J. Zhang, K. Ran, J.-M. Zuo, S. Mishina, and T. Aoki, *Microsc. Microanal.* **16**, 183 (2010).
- [16] See Supplemental Material at <http://link.aps.org/supplemental/10.1103/PhysRevB.90.180504> for the fine structures of O-K edge, bond angles, and bond length between Fe ions.
- [17] H. Hu, J.-M. Zuo, M. Zheng, J. N. Eckstein, W. K. Park, L. H. Greene, J. Wen, Z. Xu, Z. Lin, Q. Li, and G. D. Gu, *Phys. Rev. B* **85**, 064504 (2012).
- [18] P. Blaha, K. Schwarz, G. K. H. Madsen, D. Kvasnicka, and J. Luitz, *WIEN2k, An Augmented Plane Wave Plus Local Orbitals Program for Calculationg Crystal Properties* (Karlheinz Schwarz, Technische Universitat, Wien, Austria, 2002).
- [19] P. E. Blöchl, *Phys. Rev. B* **50**, 17953 (1994).
- [20] G. Kresse and J. Furthmüller, *Comput. Mater. Sci.* **6**, 15 (1996).
- [21] J. P. Perdew, K. Burke, and M. Ernzerhof, *Phys. Rev. Lett.* **77**, 3865 (1996).
- [22] V. P. S. Awana, A. Pal, A. Vajpayee, B. Gahtori, and H. Kishan, *Physica C* **471**, 77 (2011).
- [23] A. Martinelli, A. Palenzona, M. Tropeano, C. Ferdeghini, M. Putti, M. R. Cimberle, T. D. Nguyen, M. Affronte, and C. Ritter, *Phys. Rev. B* **81**, 094115 (2010).
- [24] S. L. Li, Clarina de la Cruz, Q. Huang, Y. Chen, J. W. Lynn, J. Hu, Y.-L. Huang, F.-C. Hsu, K.-W. Yeh, M.-K. Wu, and P. Dai, *Phys. Rev. B* **79**, 054503 (2009).
- [25] F. Ma, W. Ji, J. Hu, Z.-Y. Lu, and T. Xiang, *Phys. Rev. Lett.* **102**, 177003 (2009).
- [26] K. Horigane, H. Hiraka, and K. Ohoyama, *J. Phys. Soc. Jpn.* **78**, 074718 (2009).
- [27] C. Fang, B. A. Bernevig, and J. Hu, *Europhys. Lett.* **86**, 67005 (2009).
- [28] G. A. Sawatzky, I. S. Elfimov, J. van den Brink, and J. Zaanen, *Europhys. Lett.* **86**, 17006 (2009).
- [29] L. Zhang, D. J. Singh, and M. H. Du, *Phys. Rev. B* **79**, 012506 (2009).
- [30] R. Viennois, E. Giannini, D. van der Marel, and R. Černý, *J. Solid State Chem.* **183**, 769 (2010).